Experimental Investigation and Numerical Simulation of Marangoni Effect Induced by Mass Transfer during Drop Formation

Zhihui Wang, Ping Lu, Yang Wang, Chao Yang, and Zai-Sha Mao
National Key Laboratory of Biochemical Engineering, Key Laboratory of Green Process and Engineering, Institute of Process Engineering, Chinese Academy of Sciences, Beijing 100190, China

DOI 10.1002/aic.14161
Published online June 26, 2013 in Wiley Online Library (wileyonlinelibrary.com)

Marangoni effect induced by interphase mass transfer plays an important role in liquid–liquid extraction and reaction processes. The interaction of Marangoni effect and interphase mass transfer during drop formation at different injection rates and different initial solute concentrations was investigated by experimental and numerical simulation. The extraction fraction was measured and the corresponding correlation was proposed. The level-set method coupled with mass-transfer equation is for the first time used to simulate the mass-transfer induced Marangoni effect during drop formation. The simulated drop volume, shape, and extraction fraction are in good accordance with experimental data. Through the numerical simulation, it is found that the mass transfer in the first mass-transfer period is the most efficient during drop formation when Marangoni convection occurs. © 2013 American Institute of Chemical Engineers *AIChE J*, 59: 4424–4439, 2013

Keywords: Marangoni effect, level-set method, drop formation, mass transfer

Introduction

Liquid–liquid extraction and reaction are important operations in petrochemical, hydrometallurgical, pharmaceutical industries, and so forth. Single liquid drops experience three stages during its life in a process unit: (1) formation, (2) free-falling or rising, and (3) coalescence. The formation stage plays an important role as the phenomenon of drop formation determines the primitive drop size, initial velocity, and mass-transfer condition of the following processes. Popovich et al.,[1] Skelland and Minhas,[2] and Lee[3] showed that noticeable mass (around 3–50%) was extracted in the drop formation stage. Sufficient knowledge about the hydrodynamics and interphase mass transfer during droplet formation is desired to design scientifically the liquid–liquid operation units and optimize the operation of existing units.

Many efforts have been dedicated to understanding the hydrodynamics of drop formation and different models for predicting the drop growth were proposed. The widely accepted models were mainly based on the surface stretch theory and the fresh elements theory or their combination. Popovich et al.[1] summarized the previous work and proposed a model for time-dependent surface area A with the assumption that the drop was a sphere growing at a steady rate

$$A=\pi d_{\mathrm{f}}^2\left(\frac{t}{t_{\mathrm{f}}}\right)^{2/3} \tag{1}$$

However, the evaluation of mass transfer during droplet formation is rather complex and there is little research on it.[4] Some experimental approaches have been developed to estimate the mass transfer during drop formation, such as extrapolating measurements to zero formation time,[5] withdrawing the drop after its formation through the same nozzle,[6] or experimenting in a short column.[7,8] The early analytical models for prediction of mass transfer during droplet formation were based on the unsteady-state diffusion theory utilizing Higbie's penetration theory. These models failed to predict in many cases that internal circulation or convection had an important effect on mass-transfer rates. Accounting for the effects of boundary curvature, the convective flow around a forming drop, and the time-dependent concentration change in the continuous phase near the drop, Walia and Vir[9] proposed a model to predict the time-dependent mass-transfer rate

$$E_{\mathrm{d}}=\frac{36}{\sqrt{21\pi}}\frac{(D_{\mathrm{Ef}}t)^{0.5}}{d}\left[1+\frac{(\pi D_{\mathrm{Ef}}t)^{0.5}}{d}\right] \tag{2}$$

where $D_{\mathrm{Ef}}=D_{\mathrm{d}}$ is the diffusion coefficient. With the composition change of the drop accounted for, they finally obtained

$$E_{\mathrm{f,d}}=E_{\mathrm{d}}-\frac{7}{8}E_{\mathrm{d}}^2+\frac{49}{72}E_{\mathrm{d}}^3-0.476E_{\mathrm{d}}^4 \tag{3}$$

Nevertheless, their model failed to represent accurately the reported experimental data[10] in the case that the nozzle Reynolds number $Re_{\mathrm{N}}>10$. Liang and Slater[10] developed a

Correspondence concerning this article should be addressed to Chao Yang at chaoyang@home.ipe.ac.cn.

circulation/diffusion model, where E_d in Eq. 3 is calculated according to the following equation

$$E_d = \beta \frac{(D_{Ef} t_f)^{0.5}}{d_f} \left[1 + \frac{(\pi D_{Ef} t_f)^{0.5}}{d_f} \right] \quad (4)$$

where β is a coefficient varying with the model assumptions which can be referred to Walia and Vir[8,9] and $D_{Ef} = k_H(D_d + D_E)$ denotes the total diffusion coefficient. Here, k_H represents a factor expressing the degree of reduction of the effectiveness of surface eddies due to presence of surfactants and $k_H = 1$ for pure systems; D_E is the pseudoeddy diffusion coefficient which represents the convective effect

$$D_E = k_E d_f^2 / t_f \quad (5)$$

where the proportionality coefficient k_E is determined by least-squares data fitting from experimental data. Nevertheless, their diffusion/circulation model showed some shortcomings when the nozzle Reynolds number ($Re_N = \rho_d u_N d_N / \mu_d$) $Re_N > 10$. Using the pseudoeddy diffusion coefficient D_E

$$D_E = \frac{d_f u_d}{2048(1 + \mu_d/\mu_c)} \quad (6)$$

$$u_d = Q/\left(\pi d_f^2/4\right) \quad (7)$$

$$D_{Ef} = D_d + D_E \quad (8)$$

proposed by Handlos and Baron[11] for a moving drop as a correction to represent the convective effect during drop formation, Lu et al.[12] calculated D_{Ef} in Eq. 2 as an addition of molecular-diffusion coefficient D_d and convective coefficient D_E by Eq. 8, and they found the extraction fraction estimated by Eq. 3 fitted well with experiments when $Re_N > 10$. Assimilating the entrance of the dispersed flow into the growing drop from the nozzle to the entrance of the flow from a smaller channel to a larger one, Javadi et al.[4] proposed a "flow expansion model" to predict interphase mass transfer

$$M_t = \text{const} \cdot \Delta c D_d Sc^{1/3} S \frac{3}{4-n} \frac{Re_N^n (R_N/u_N)^{(n+1)} t_f^{(4-n)/3}}{R_N} \quad (9)$$

where M_t is the cumulative mass transfer during droplet formation, $Sc = \mu_d/(\rho_d D_d)$, $Re_N = \rho_d u_N d_N/\mu_d$, and $S = 10.37 (u_N R_N^2 t)^{2/3}$. n is a constant between 0.33 and 1.2 related to the convection within the droplet. This model showed better agreement with the experimental data by Zimmermann et al.[13] than Liang and Slater's circulation/diffusion model.[10]

The interfacial instability due to interfacial tension gradient induced by variation of temperature or solute concentration along the interface, called "Marangoni effect," occurs frequently during heat or mass transfer from/to droplets. Abundant experimental results indicated that Marangoni effect could enhance transport rates efficiently.[14,15] Flow visualization, analysis of variation of transport rates, and the combinations of both approaches are efficient to identify occurrence of Marangoni effect. For thermocapillary convections, Schwabe et al.[16] used neutrally buoyant tracer particle accumulation to reveal the convection features in floating zones under microgravity. Schwabe[17] visualized the Benard–Marangoni instability using aluminum flakes that oriented parallel to the streamlines. Because of the nonintrusiveness, optical measurement techniques allow measurements without disturbance of mass transfer and fluid dynamics. Schlieren optical technique is commonly adopted to visualize the interfacial convection induced by mass transfer. Assembling a conventional Schlieren-Toepler optical arrangement[18] with two achromatic field lenses, Okhotsimskii and Hozawa[19] visualized the variety of flow patterns of the coupled Marangoni and Rayleigh convection. Lohner et al.[20] combined the rainbow refractometry and Schlieren optical measurements to detect occurrence of Marangoni effect. Agble and Mendes-Tatsis[21] applied the Schlieren optical technique and Mach–Zehnder interferometer, respectively, to observe the interfacial phenomena and measure the mass-transfer rate of organic drops stagnant in surfactant aqueous solutions.

To define quantitatively the relation between mass-transfer rate and Marangoni effect, many elaborate works have been done. Arendt et al.[22] applied Schlieren optical technique to detect Marangoni effect and a three-mode magnetic suspension balance connected to an optical cell to analyze the mass transfer in the process of CO_2 transport over planar interface. On the basis of penetration theory and the experimental findings of Hozawa et al.,[23] they proposed an empirical equation to calculate the additional mass-transfer coefficient due to Marangoni convection at a flat interface

$$k_M = \sqrt{\frac{D_d}{\pi t}} \frac{\sigma_{ref}}{\sigma} \quad (10)$$

Taking the similar experimental approach, Marangoni convection was found to occur only in case of the transfer direction of solute acetone from the pendant water droplet into the continuous toluene phase.[14] They found that good agreement of the experimental results with the calculation from Kronig and Brink models,[24] with the deviation less than 15% for a pendant drop with the inner circulation dominated by the Rayleigh effect. Furthermore, accounting for the effect of interface shape, Arendt and Eggers[14] augmented Eq. 10 to the following formula

$$k_M = \sqrt{\frac{D_d}{\pi t}} \frac{\sigma_{ref} - \sigma_{eq}}{\sigma_{ref}} \frac{L_{ref}}{L} \quad (11)$$

to describe the contribution of Marangoni convection separately in addition to Rayleigh effect. The linear superposition of Kronig and Brink[24] model and Eq. 11 made the deviation from experimental data less than 10%. Wang et al.[25] detected the Marangoni effect when acetic acid was transferred from a hanging 1-hexanol droplet to the continuous water phase and found that the mass-transfer rate can be predicted by Kronig and Brink[24] circulating model with proper eigenvalues.

However, the experimental work on Marangoni effect induced by mass transfer during drop formation period was scarcely reported. On the basis of capillary pressure experiments and a new flow expansion model[4] proposed for the mass transfer of a growing drop, Javadi et al.[26] examined the

effect of liquid flow rate, capillary diameter, droplet size, and so forth, on the possibility and strength of Marangoni instability. They found that the overall mass-transfer coefficient ratio of two phases, which included both diffusive and convective effects, turned out to be the key parameter for predicting interfacial instability of growing drops. For a uniformly growing spherical drop, Popovich et al.[1] advanced the following model

$$M=\text{const}\cdot d_{\mathrm{f}}^2\Delta c\sqrt{\pi t_{\mathrm{f}}D_{\mathrm{d}}} \tag{12}$$

where $\Delta c=c_0-c^*$, c_0 is the initial solute concentration in the dispersed phase, c^* is the concentration in equilibrium with the concentration of the continuous phase. On the basis of Eq. 12, Wegener et al.[27] used a coefficient ($\alpha(c_0)$) correlated to initial solute concentration to predict the transferred mass during drop formation period in the ternary system toluene/acetone/water with Marangoni effect by

$$M=\frac{6}{7}d_{\mathrm{f}}^2\Delta c\sqrt{\pi t_{\mathrm{c}}}\sqrt{\alpha(c_0)D_{\mathrm{d}}} \tag{13}$$

where t_c is the sum of the drop formation time, the time between the end of formation and release (0.2 s), and the withdrawal time when the dispersed phase withdrawn by pump. Compared to their experimental results, the predictions were satisfactory with the error less than $\pm 30\%$. Nevertheless, they experimented on one system only, the relationship between $\alpha(c_0)$ and the initial concentration was different when the solute transported in different directions.

The numerical works on thermocapillary Marangoni effects were reported quite frequently, for example, thermocapillary migration of bubbles[28–30] and drops[31–35] and liquid-bridge instability.[36–39] In contrast, fewer numerical simulations were conducted on the mass-transfer induced Marangoni effect, and most researches were focused on liquid layers.[40–45] Lee et al.[40] reported the Marangoni convection at gas–liquid interface induced by surfactant absorption into falling liquid film. Schott and Pfennig[46] modeled the Marangoni effect induced by mass transfer at liquid/liquid interface based on molecular simulation. Grahn[42] conducted two-dimensional (2-D) simulations of isothermal liquid/liquid mass transfer subject to surface tension and buoyancy-driven hydrodynamic instabilities and showed formation of roll cells and plume-like convective structures already known from experimental observations. Mao et al.[44] conducted a 2-D simulation on the mass-transfer induced Marangoni effect in a two liquid layer system. Numerical researches of the drop Marangoni instability induced by mass transfer were mainly focused on drop moving stage.[47–49] Mao and Chen[47] studied numerically in axisymmetric simulations the influence of Marangoni effect on mass transfer of a slowly moving drop in a liquid–liquid system using boundary fitted coordinates. Wegener et al.[50] simulated the fluid dynamics and mass-transfer process of a moving drop with Marangoni instability via the commercial computational fluid dynamics (CFD)-code STAR-CD under the assumption of a spherical drop. Wang et al.[48] formulated the mathematical model of mass-transfer induced Marangoni effect with the interface captured by the level-set method and studied numerically the impact of Marangoni effect on mass transfer of an accelerating axisymmetric deformable drop.[49]

Several numerical investigations[51–57] on the dynamics of drop formation without mass transfer have been reported. Gerlach et al.[53] and Buwa et al.[54] applied a combined level set and volume of fluid (VOF) method to simulate the bubble formation, and the prediction of bubble growth and shape agreed well with experimental data. Soleymani et al.[55] used the VOF method to simulate drop formation in a solvent extraction system. Yang et al.[57] simulated the formation process of a single drop in an immiscible liquid or gas phase by the level-set method. Lu et al.[12] used the level-set method to capture the interface and instantaneous concentration during drop formation by solving the coupled motion/mass transfer equations. Although the predicted drop formation time and mass-transfer fraction agreed well with experimental results at high-formation speeds, the volume loss increased with the decrease of formation speed (900, 600, and 400 μL/min). Numerical simulation of the mass transfer during drop formation especially at lower formation rates needs to be improved to guarantee mass conservation. To date, there is no report on numerical simulation of Marangoni effect induced by mass transfer during drop formation.

In this work, the experiments on mass transfer of solute acetic acid or acetone from single 1-hexanol drops to continuous water phase and acetic acid from methyl isobutyl ketone (MIBK) drops to water were carried out. Accounting for the impact of Marangoni effect on mass transfer, a correlation to calculate the extraction fraction during drop formation with Marangoni effect was proposed. With a modified mass-amending method embodied in the numerical program, the simulation of Marangoni effect induced by mass transfer during drop formation by the level-set approach was conducted. The behavior of interfacial convection and interphase mass transfer was interpreted with the flow field detailed by numerical simulation.

Experimental Section

Materials

Three extraction systems, 1-hexanol (drop phase)/acetic acid (solute)/water (continuous phase), 1-hexanol (dispersed phase)/acetone/water (continuous phase), and MIBK (drop phase)/acetic acid/water (continuous phase), were used in our experiments. The drop phases of 1-hexanol and MIBK are analytical reagents ($\geq$98.5%) from Sinopharm Chemical Reagent, China. The continuous phase is deionized water. The solutes of acetone and acetic acid are analytical reagents ($\geq$99.5%) from Beijing Chemical Reagent. The physical properties of above systems are listed in Table 1. The distribution coefficient m of acetic acid between MIBK and water and the interfacial tension of MIBK/acetic acid/water system have been given by Misek.[59] The distribution coefficient m of acetone or acetic acid between 1-hexanol and water was measured as shown in Figure 1a. The interfacial tensions of 1-hexanol/acetone/water and 1-hexanol/acetic acid/water systems were measured by an interfacial tension analytical instrument (FTA200, First Ten Angstroms). The relationships of interfacial tension σ with solute concentration in 1-hexanol/water system are shown in Figure 1b. m and σ of three systems can be estimated by the following correlations resulted from least-squares data fitting

MIBK/acetic acid/water

$$m=0.587+0.141c-0.0140c^2 \tag{14a}$$

$$\sigma=9.915-5.022c+0.785c^2 \tag{14b}$$

Table 1. Physical Properties of Extraction System Components at 25°C

Material	ρ (kg/m^3)	μ (mPa·s)	D_d (10^{-9} m^2/s)	D_c (10^{-9} m^2/s)
Water (continuous phase)	997.3	0.89		
MIBK (drop)	796.1	0.542		
1-hexanol (drop)	813.6	4.44		
Acetic acid (solute)	1043.7	0.1229	≈ 0.39 (1-hexanol)[58] 1.43 (MIBK)	1.04
Acetone (solute)	784.4	0.304	0.41	1.15

1-hexanol/acetone/water

$$m=0.803+0.105c+0.507c^2 \quad (15a)$$

$$\sigma=5.399-0.235\ln(c-0.00107) \quad (15b)$$

1-hexanol/acetic acid/water

$$m=0.774+0.411c-0.422c^2 \quad (16a)$$

$$\sigma=6.76-3.595c \quad (16b)$$

where the unit of c is mol/L and that of σ is mN/m.

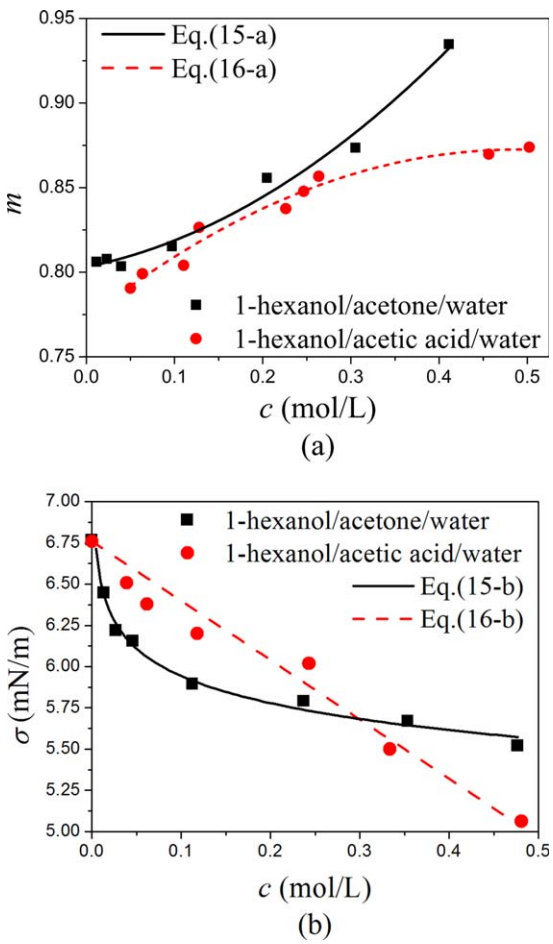

Figure 1. Distribution coefficient (a) and interfacial tension (b) in 1-hexanol/acetic acid/water and 1-hexanol/acetone/water systems.

[Color figure can be viewed in the online issue, which is available at wileyonlinelibrary.com.]

Experimental procedure

The experimental setup is the same as that built up for a hanging drop.[25] The detailed setup of the transparent quartz glass extraction cell can be referred to our previous work.[12] A Schlieren optical system combined with a CCD camera (Model 902B, 60 frames/s, Watec) was set up to capture continuously the drop motion and the interfacial convection of single drops in the formation stage. To obtain the drop outline and calculate the volume of each drop at different instants, the images were analyzed by software FTÄ 32 (First Ten Angstroms). The detailed procedure to measure mass transfer and minimize the coalescence effect was detailed in Lu et al.[12] The extraction fraction during the formation stage was calculated by

$$E_f=\frac{c_0-c_f}{\Delta c} \quad (17)$$

where $\Delta c=c_0-c^*=c_0$, because the concentration in the vast continuous phase was supposed to keep at a nearly zero level.

Lu et al.[12] have measured the extraction fraction at the end of drop formation when acetic acid transferred from MIBK drops to water under the condition that no Marangoni instability was observed. Their data presented in Figure 2 indicate that the extraction fraction estimated by Eq. 3 with the convective effect considered in calculation of the effective diffusion coefficient as Eq. 8 ($D_{Ef}=D_d+D_E$) fitted better to experiments than that considering only molecular diffusion coefficient ($D_{Ef}=D_d$), no matter Re_N greater than 10 or not. Therefore, with reference to $E_{f,d}$ which is the extraction fraction during drop formation when no Marangoni effect happens estimated by Eq. 3 with $D_{Ef}=D_d+D_E$, the mass transfer enhanced by Marangoni instability can be signified by an enhancement factor F, which could be calculated as follows

$$F=E_f/E_{f,d} \quad (18)$$

Experimental results

As presented in Figure 3, the enhancement factor is higher than one in most cases, which indicates that the Marangoni instability manifests itself in the investigated systems. We use hollow symbols to indicate the cases without Marangoni convection and solid symbols for the cases with Marangoni convection observed, and all experimental cases are listed in Tables 2 and 3. As the ability of acetone to reduce the interfacial tension of 1-hexanol/water system is greater than that of acetic acid when the concentration is less than 0.1 mol/L (Figure 1b), the enhancement factor F of acetone is larger than that of acetic acid under similar initial concentrations. For most experiments, F increases with the decline of

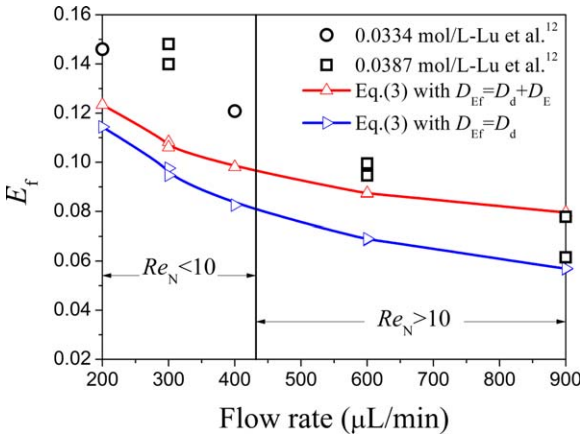

Figure 2. Experimental and predicted extraction fractions in MIBK/acetic acid/water at 20°C as a function of flow rate.

[Color figure can be viewed in the online issue, which is available at wileyonlinelibrary.com.]

formation rate and the increase of initial solute concentration, which complies with the trend of development of Marangoni convection (Figures 4 and 5). Through the capillary pressure measurements, Javadi et al.[26] found the same trend that the intensity of Marangoni turbulence decreased with increasing formation rate. For the same initial concentration, the solute would be taken away faster from the interface by stronger bulk flows at higher formation rates. Hence, the concentration difference at the interface is hard to be built up to give enough driving force to initiate and, furthermore, maintain the Marangoni instability. An exception is detected in 1-hexanol/acetic acid/water system at $c_{HAC,d} = 0.132$ mol/L, where $F = 2.99$ at $Q = 12$ μL/min is lower than $F = 3.58$ at $Q = 60$ μL/min. However, the extraction fraction $E_f = 61.3\%$ at $Q = 12$ μL/min is higher than $E_f = 36.4\%$ at $Q = 60$ μL/min, which implies that more solutes are extracted at $Q = 12$ μL/min. With the proceeding of mass transfer, the average concentration and local concentration difference at the interface decrease, which leads to the diminished drive force for Marangoni convection, and the strength of interfacial convection would be consequently weakened. The interfacial convection is observed to ebb obviously when $t > 0.8\ t_f$. As a result, the average strength of interfacial instability during the whole drop formation process is slackened down and the mass-transfer enhancement factor declines accordingly.

Correlation

So far, only Wegener et al.[27] proposed a correlation, Eq. 13, for the extracted mass during drop formation stage in the ternary toluene/acetone/water system where Marangoni convection occurred. If the transferred mass calculated by Eq. 13 is divided by the maximum possible transferred mass $V_f \Delta c$, the extraction fraction of a drop with Marangoni effect during the formation period can be obtained as follows

$$E_f = \frac{6}{7}\sqrt{\alpha(c_0)\pi}\sqrt{Fo} \tag{19}$$

where $\alpha(c_0)$ is an initial concentration-dependent diffusivity factor, accounting for the additional convection effect due to Marangoni effect, which can be obtained by regression analysis of experimental data. The Fourier number $Fo = tD_{Ef}/d_f^2$, where t is the contact time t_c and $D_{Ef} = D_d$. According to Wegener et al.[27] $\alpha(c_0) = 181.268c_0 + 0.204$ when acetone transferred from a toluene drop to water and $\alpha(c_0) = 27.646c_0 + 3.55$ when acetone transferred in the reverse direction (the inner diameter of the glass nozzle d_{in} is 0.5 mm). In their work, the contact time t_c is about two to three times of the formation time t_f.

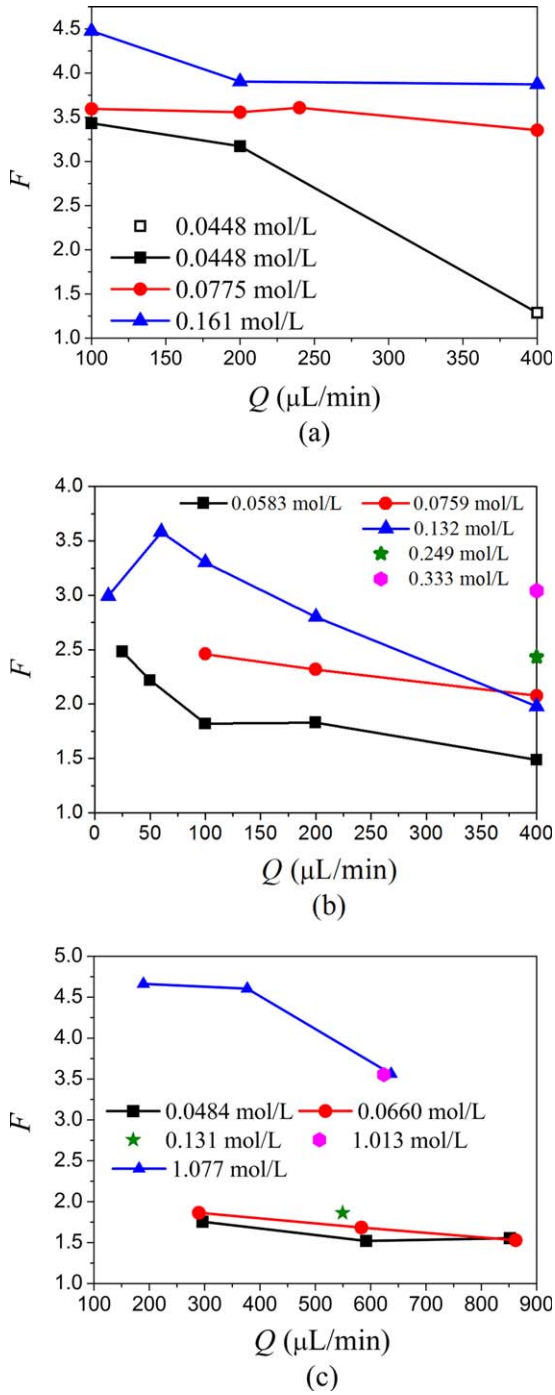

Figure 3. Enhancement factors at different solute concentrations: (a) 1-hexanol/acetone/water; (b) 1-hexanol/acetic acid/water; and (c) MIBK/acetic acid/water.

[Color figure can be viewed in the online issue, which is available at wileyonlinelibrary.com.]

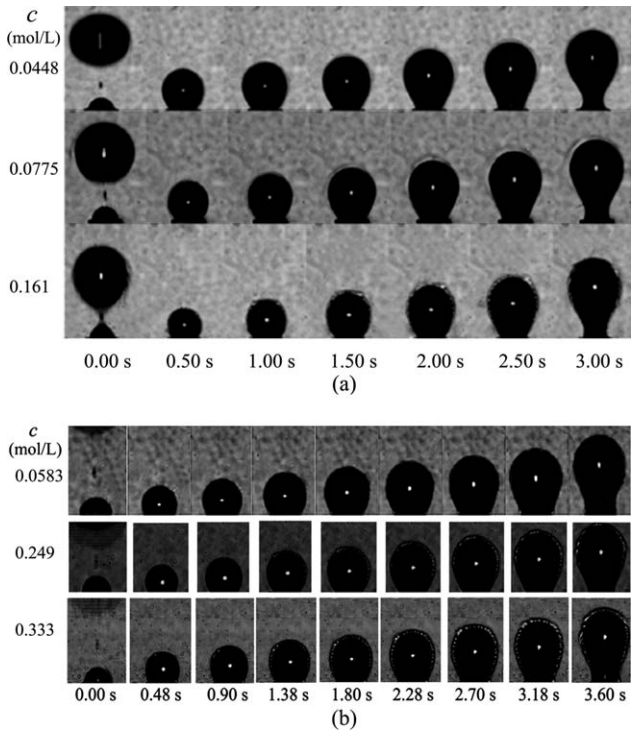

Figure 4. Effect of solute concentration on Marangoni convection ($Q = 200$ μL/min): (a) 1-hexanol/acetone/water and (b) 1-hexanol/acetic acid/water.

In experiment of this work, the time between release of the drop from the needle and arrival at the collecting funnel neck is in the range of 0.40–0.45 s, which is much shorter than the formation time. For calculation simplicity, we substitute t_f for t_c in calculation of Fo. As shown in Figure 6, the following equation fits well with experiments, where $\alpha(c_0)$ and E_c for different systems are listed in Table 4.

$$E_f = \frac{6}{7}\sqrt{\alpha(c_0)\pi}\sqrt{Fo} + E_c \tag{20}$$

The fact that Eq. 20 with $\alpha(c_0)$ fits well with experiments suggests that Marangoni effect does make significant influence on the mass transfer during drop formation. Because the properties of systems are different, the diffusivity factors $\alpha(c_0)$ cannot be expressed as a unified function of c_0 for different systems. Accounting for the influences of viscosity ratio, drop geometry configuration and Marangoni effect, we obtain a more general correlation (Eq. 21) to estimate the extraction fraction of the solute from a drop to the continuous phase with Marangoni convection taking place (the end effect of drop coalescence included)

$$E_{f,tot} = 0.0623 Ma^{0.3995}\left(\frac{d_N}{d_f}\right)^{0.6304}\left(\frac{\mu_d}{\mu_c}\right)^{0.2587}\sqrt{Fo} - 0.04338 \tag{21}$$

where the Marangoni number is $Ma = d_f\Delta\sigma/(\mu_d D_d)$ and D_{Ef} in F_O is calculated by Eq. 8 to account for the convective effect caused by the drop formation rate. As shown in Figure 7, for the systems listed in Tables 2 and 3, most of calculated data by Eq. 21 coincide with experimental measurements within 30%. The larger deviation in 1-hexanol/acetone/water system may be due to longer coalescence

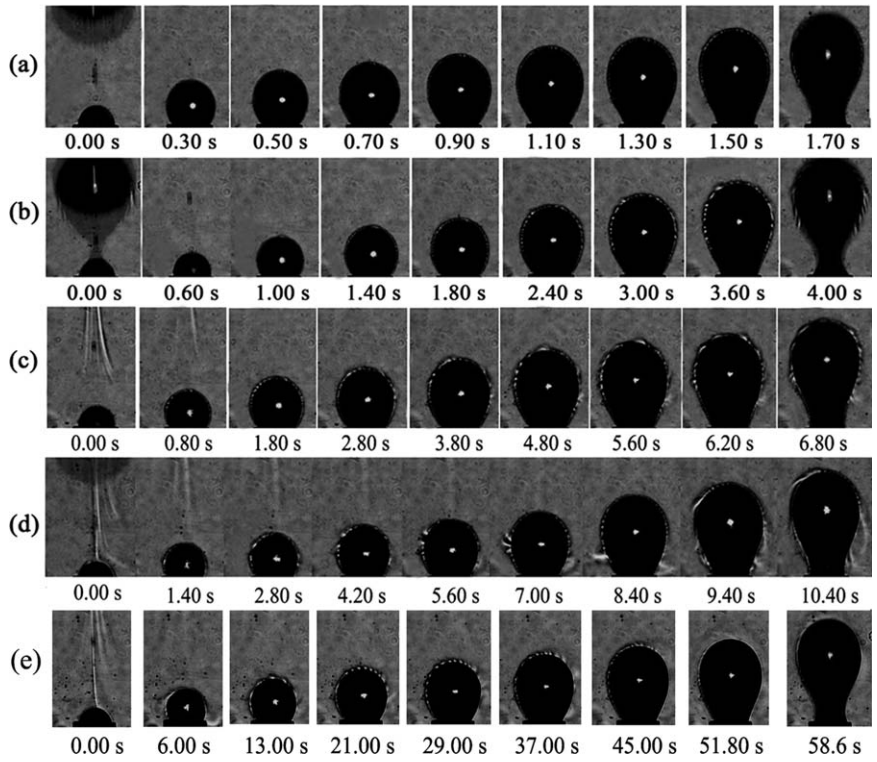

Figure 5. Interfacial phenomena in 1-hexanol/acetic acid/water system at different inject flow rates ($c_{HAC,d} = 0.132$ mol/L): (a) $Q = 400$ μL/min; (b) $Q = 180$ μL/min; (c) $Q = 100$ μL/min; (d) $Q = 50$ μL/min; and (e) $Q = 12$ μL/min.

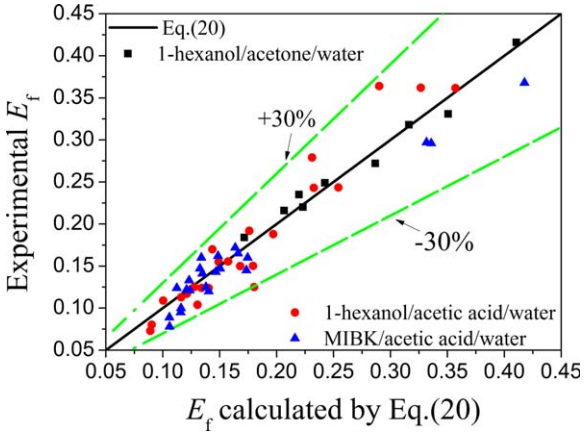

Figure 6. Comparison of experimental data with calculated extraction fraction by Eq. 20.

[Color figure can be viewed in the online issue, which is available at wileyonlinelibrary.com.]

processes at the funnel neck as observed during our experiments.

Numerical Simulation and Discussion

Mathematical modeling

In this work, a mathematical model of an axisymmetric liquid drop growing in another immiscible continuous phase under gravity is built up, in which the mass-transfer induced Marangoni effect is taken into consideration. To simplify the model, the following assumptions are made: (1) the drop shape is axisymmetric; (2) the two fluids are viscous, Newtonian, and incompressible; (3) the flow is isothermal and axisymmetric; (4) the flow is laminar even if disturbed locally by the Marangoni convection of inherent 3-D nature; and (5) the variation of solute concentration due to mass transfer has no effect on the physical properties of the system except interfacial tension.

The level-set function $\phi(\mathbf{x},t)$ is defined as the outward normal distance from the drop surface. The following Hamilton–Jacobi type equation is used to advance the interface[12]

$$\frac{\partial \phi}{\partial t}+\nabla\cdot(\mathbf{U}\phi)=0 \tag{22}$$

The continuity and Navier–Stokes equations with the evolving surface tension incorporated are adopted to describe the two-phase flow with Marangoni effect[49]

$$\nabla\cdot\mathbf{U}=0 \tag{23}$$

$$\rho\left(\frac{\partial \mathbf{U}}{\partial t}+\mathbf{U}\cdot\nabla\mathbf{U}\right)=-\nabla P+\rho\mathbf{g}+\nabla\cdot\left(\mu\left(\nabla\mathbf{U}+\nabla\mathbf{U}^{\mathrm{T}}\right)\right)+\mathbf{F}_{\mathrm{Ma}} \tag{24}$$

where the source term $\mathbf{F}_{\mathrm{Ma}}$ generated by the surface-tension gradient inducing Marangoni effect is modeled by the well-known continuum surface force model[60]

$$\mathbf{F}_{\mathrm{Ma}}(\mathbf{x})=(\sigma\kappa\mathbf{n}+\nabla_s\sigma)\delta(\mathbf{x}-\mathbf{x}_s) \tag{25}$$

where $\mathbf{x}_s$ is the point on the interface, δ is the Dirac delta function, and σ is the interfacial tension which can be correlated to the solute concentration according to Figure 1 $\kappa=-\nabla\cdot\mathbf{n}$ and $\mathbf{n}=-\nabla\cdot(\nabla\phi/|\nabla\phi|)$. To manifest the real interfacial convection induced by Marangoni effect, the weighted integration method[61] for calculating accurately the surface-tension force at the interface nodes is incorporated to suppress the parasitic flow.

The "one fluid" mass-transfer formulation[62] is used

$$\frac{\partial \hat{c}}{\partial \hat{t}}+\hat{\mathbf{U}}\cdot\nabla\hat{c}=\hat{D}\nabla^2\hat{c} \tag{26}$$

The definition of the variables and the detailed derivation of above equations in level-set approach can be referred to Yang and Mao.[62]

The algorithm for the level-set function is in a nonconservative form. Lu et al.[12] used the reinitialization method of level-set function in Eq. 27 proposed by Sussman et al.[63] to amend the volume loss

$$\frac{\partial \phi}{\partial \tau}=\mathrm{sgn}\,(\phi_0)(1-|\nabla\phi|) \tag{27}$$

where ϕ_0 is a level-set function at an instant of real time and $\mathrm{sgn}\,(\phi_0)$ denotes the smoothed sign function with appropriate numerical smearing to avoid any numerical difficulties. They found that the drop volume loss could reach even up to 17%.

In this work, in addition to the above reinitialization method,[63] another mass-amending method by solving Eq. 28 proposed by Chang et al.[64] and modified by Yang and Mao[65] is adopted to guarantee the mass conservation during drop formation

$$\frac{\partial \phi}{\partial \tau}+(A_0-A(\tau))(-P+\kappa(\phi))|\nabla\phi|=0 \tag{28}$$

where τ is the virtual time, typically P can be set to be one,[66] A_0 stands for the mass of a fluid particle at $\tau=0$, and according to Yang and Mao,[65] $A(\tau)$ is the mass of a fluid particle corresponding to the level-set function $\phi(\tau)$

$$A(\tau)=\sum_{\phi_{ij}\le\varepsilon}\rho_\varepsilon(\phi_{ij})r_j\Delta x\Delta y \tag{29}$$

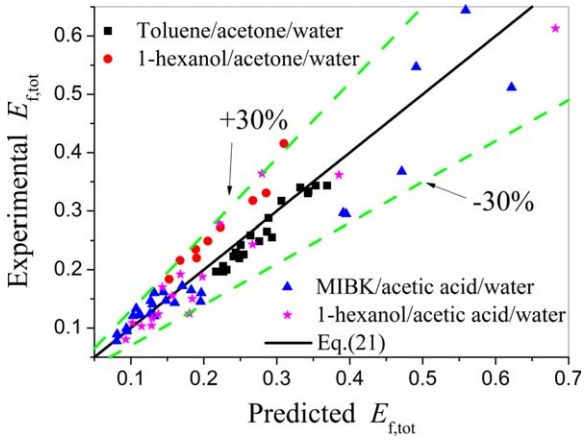

Figure 7. Comparison of experimental data with calculated extraction fraction by Eq. 21.

[Color figure can be viewed in the online issue, which is available at wileyonlinelibrary.com.]

Table 2. Experimental Mass Transfer Data (Solute: Acetone)

Experiment	C_0 (mol/L)	t_f (s)	d_f (mm)	$Ma \times 10^{-7}$	D_{Ef} (10^{-9} m^2/s)	E_f	MC
Toluene /water[27] (d_N = 1.19 mm)	0.0646	0.65	1.988	0.538	4.034	0.229	Yes
		1.06	2.506	0.678	4.003	0.200	Yes
		1.48	3.009	0.814	4.043	0.197	Yes
		2.42	3.481	0.942	3.815	0.197	Yes
		3.47	3.984	1.082	3.734	0.207	Yes
	0.129	0.65	2.019	0.669	4.075	0.259	Yes
		1.06	2.506	0.831	4.005	0.226	Yes
		1.48	2.994	0.993	4.032	0.223	Yes
		2.42	3.497	1.159	3.826	0.219	Yes
		3.47	3.984	1.321	3.728	0.242	Yes
	0.258	0.65	2.003	0.896	4.058	0.317	Yes
		1.06	2.506	1.122	4.008	0.255	Yes
		1.48	3.009	1.347	4.048	0.249	Yes
		2.42	3.497	1.565	3.828	0.265	Yes
		3.47	3.984	1.783	3.730	0.288	Yes
	0.516	0.65	1.988	1.305	4.045	0.344	Yes
		1.06	2.490	1.635	3.998	0.344	Yes
		1.48	2.994	1.966	4.041	0.340	Yes
		2.42	3.497	2.296	3.834	0.330	Yes
		3.47	4.000	2.627	3.742	0.337	Yes
1-hexanol/water (d_N = 1.19 mm)	0.0448	1.714	2.795	0.116	0.681	0.0693	No
		3.334	2.741	0.114	0.548	0.220	Yes
		6.920	2.787	0.116	0.478	0.318	Yes
	0.0775	1.646	2.735	0.169	0.683	0.184	Yes
		2.748	2.759	0.170	0.552	0.235	Yes
		3.443	2.799	0.172	0.480	0.249	Yes
		6.916	2.742	0.169	0.691	0.331	Yes
	0.161	1.844	2.864	0.142	0.577	0.216	Yes
		3.294	2.758	0.137	0.547	0.272	Yes
		6.818	2.790	0.139	0.480	0.416	Yes

Ma is Marangoni number defined as $Ma = d_f \Delta\sigma/(\mu_d D_d)$; MC stands for Marangoni convection.

where $\phi_{ij} \leq \varepsilon$ denotes the nodes in a fluid particle and the interface in a virtual thickness of 2ε, and the density is smoothed by the regularized Heaviside function $H_\varepsilon(\phi_{ij})$ as $\rho_\varepsilon(\phi_{ij}) = \rho_d/\rho_c + (1-\rho_d/\rho_c)H_\varepsilon(\phi_{ij})$. The mass-amending method incorporated Eq. 27 with Eq. 28 was verified in simulation of a deformable moving drop with Marangoni effect.[49] For a growing drop, there is a mass source $A_{in} = \rho_d Qt$ at the inlet. Therefore, A_0 in Eq. 28 should be calculated by

$$A_0 = A_{t=0} + A_{in} \tag{30}$$

The discretization of Eq. 28 can be referred to Yang and Mao.[65] The algorithm for other equations has been detailed by Lu et al.[12] The computational procedure is as follows:

Step 1. Initialize the flow field, physical parameters and ϕ as signed normal distance to the interface;
Step 2. Solve Eqs. 23 and 24 for one time step;
Step 3. Solve the concentration field by Eq. 26;
Step 4. Update level-set function ϕ by Eq. 22;
Step 5. Reinitialize ϕ by solving Eqs. 27 and 28 successively to steady state;
Step 6. Repeat steps 2–5 till the designated time.

Validation of numerical simulation

As the extraction cell and mass-transfer procedure in our experiments are the same as that detailed by Lu et al.,[12] the computational domain (40*R* in *x* direction and 15*R* in *y* direction) and mesh independence test are also the same as the previous work. The nonuniform grid with 185 × 72 nodes (meshes in *x* and *y* directions, respectively) is sufficient for spatial computational accuracy.

All numerically simulated cases in 1-hexanol/acetic acid/water system are listed in Table 5. As indicated by Figure 8, the simulated transient drop volume by the numerical model incorporated with Eq. 28 matches much better with the experimental observation at the corresponding time instants than that only by Eq. 27. Even at very slow formation rate Q = 100 μL/min, the average relative deviation between the simulated drop volumes and the experimental data is still less than 9%. Furthermore, the predicted drop shapes under different formation rates (Q = 100 and 200 μL/min) are in very good agreement with experimental images (Figure 9) and the relative deviation of the detachment time is less than 5%.

As the interfacial tension is set to be 5.51 mN/m (at $c_{HAC,d}$ = 0.333 mol/L), the velocity vector and streamlines presented in Figure 10 do not show any obvious parasitic flow at the interface, indicating that the present numerical model generates no parasite flow and the possible Marangoni effect would not be masked. As shown in Figure 11, the simulated extraction fraction during the formation period before the neck formation fits well with Walia and Vir's prediction,[9] and after detachment E_f is in good accordance with Eq. 3 when the effective diffusion coefficient is calculated by Eq. 8.

Marangoni effect and mass transfer during drop formation

As shown in Table 5, most of the simulated E_f is lower than that calculated by Eq. 27, because Eq. 27 is obtained according to the experiments where E_f is the average value of about 15 drops and the mass transfer during coalescence is included. The predicted average E_f of five drops is 0.15 at c_0 = 0.333 mol/L and higher than the measured E_f = 0.14 of the first drop, which may be due to the strength of Marangoni convection when a followed drop formed from the fore

Table 3. Experimental Mass Transfer Data (Solute: Acetic Acid)

Experiment	C_0 (mol/L)	t_f (s)	d_f (mm)	$Ma \times 10^{-6}$	D_{Ef} (10^{-9} m^2/s)	E_f	MC
MIBK/water (d_N = 1.19 mm)	0.0334	5.95	3.301	0.660	1.788	0.147	No
		3.30	3.487	0.697	2.159	0.121	No
	0.0387	4.00	3.280	0.759	1.959	0.120	No
		2.014	3.357	0.777	2.541	0.095	No
		1.379	3.379	0.782	3.079	0.089	No
		4.125	3.436	0.795	1.994	0.125	No
		2.164	3.460	0.801	2.528	0.100	No
		1.490	3.500	0.810	3.067	0.078	No
	0.0484	4.150	3.395	0.979	1.977	0.162	Yes
		2.167	3.443	0.993	2.515	0.133	Yes
		1.450	3.400	0.980	3.016	0.124	Yes
	0.0660	4.033	3.337	1.302	1.973	0.172	Yes
		1.950	3.308	1.291	2.542	0.147	Yes
		1.467	3.427	1.338	3.020	0.122	Yes
	0.0680	2.067	3.376	1.369	2.522	0.141	Yes
	0.0716	1.683	3.153	1.331	2.600	0.160	Yes
	0.131	2.150	3.350	2.517	2.531	0.165	Yes
	0.158	2.133	3.395	3.049	2.458	0.160	Yes
		2.050	3.363	3.020	2.493	0.145	Yes
	1.013	1.683	3.221	12.605	2.515	0.297	Yes
	1.077	5.383	3.189	12.881	2.553	0.512	Yes
		2.667	3.175	12.825	1.766	0.368	Yes
		1.600	3.189	12.881	2.580	0.295	Yes
	2.745	1.930	2.759	13.240	2.017	0.644	Yes
		1.367	2.773	13.308	2.270	0.547	Yes
1-hexanol/water (d_N = 1.19 mm)	0.0524	1.814	2.797	0.587	0.678	0.0634	No
		3.702	2.775	0.582	0.520	0.104	Yes
		6.991	2.761	0.579	0.462	0.125	Yes
	0.0583	1.962	2.791	0.603	0.622	0.083	Yes
		3.703	2.798	0.605	0.540	0.117	Yes
		6.992	2.757	0.596	0.474	0.150	Yes
		13.39	2.773	0.599	0.440	0.243	Yes
		25.71	2.736	0.591	0.423	0.362	Yes
	0.0759	1.812	2.748	0.698	0.646	0.109	Yes
		3.725	2.753	0.699	0.519	0.170	Yes
		7.014	2.760	0.701	0.462	0.188	Yes
	0.132	1.752	2.751	0.881	0.655	0.103	Yes
		4.006	2.745	0.879	0.510	0.192	Yes
		6.903	2.744	0.879	0.463	0.279	Yes
		10.91	2.748	0.880	0.439	0.364	Yes
		60.13	2.773	0.888	0.405	0.613	Yes
	0.249	1.952	2.710	0.994	1.291	0.124	Yes
	0.333	1.953	2.710	1.069	1.667	0.155	Yes

Ma is Marangoni number defined as $Ma = d_f \Delta\sigma/(\mu_d D_d)$; MC stands for Marangoni convection.

Table 4. Coefficients in Eq. 20 for Different Systems

System	$\alpha(c_0)$	E_c
1-hexanol/acetone/water	$758.931c_0+93.47$	0
1-hexanol/acetic acid/water	$314.062c_0+22.1$	0
MIBK/acetic acid/water	$136.073c_0$	0.06

detached drop was stronger than the first fresh one (Javadi et al.[26] found the same phenomena in their pressure measurement). Eliminating the additional mass transfer, Eq. 31 fits well with the simulated extraction fraction of the first fresh drop (Figure 12)

$$E_{f,det} = E_{f,tot} - 0.02859 = 0.0623 Ma^{0.3995} \left(\frac{d_N}{d}\right)^{0.6304} \left(\frac{\mu_d}{\mu_c}\right)^{0.2587} \sqrt{Fo} - 0.07197 \quad (31)$$

Figure 12a shows the transient extraction fractions at different initial concentrations of 0.0583, 0.249, and 0.333 mol/

Table 5. Numerical Simulation Cases of 1-hexanol(d)/acetic acid/water(c) System

c (mol/L)	Q (μL/min)	σ (mN/m)	Re_N	m	$E_{f,det}$ (sim.)	$E_{f,tot}$ (exp.)	$E_{f,tot}$ (pred.)	ME
0.0583	100	6.38	0.358	0.800	0.1668	0.150	0.166	Y
	200	6.38	0.716	0.800	0.0926	0.117	0.147	Y
	366	6.38	1.310	0.800	0.0767	0.0830	0.0994	Y
0.249	366	5.86	1.386	0.865	0.108	0.124	0.130	Y
0.333	366	5.51	1.387	0.884	0.140	0.155	0.185	Y
0.333	366	5.51	1.387	0.884	0.0562		0.0530	N

ME stands for Marangoni effect, Y means Marangoni effect is considered in the simulation, and N means Marangoni effect is not considered (interfacial tension is taken constant); $E_{f,tot}$ is calculated by Eq. 21 for the cases accounting for Marangoni effect or by Eq. 3 with $D_{Ef} = D_d + D_E$ for the case without Marangoni effect.

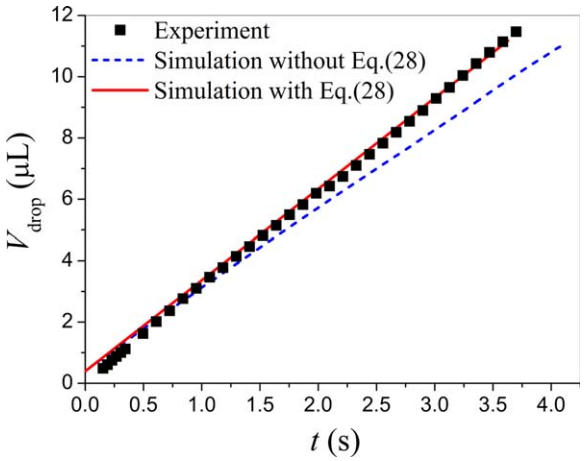

Figure 8. Comparison of drop volumes during drop formation ($c_{HAC,d}$ = 0.0583 mol/L, Q = 200 μL/min).

[Color figure can be viewed in the online issue, which is available at wileyonlinelibrary.com.]

L as the drop formation rate was kept at 366 μL/min. Figure 12b presents the evolution of the extraction fractions at different formation rates with initial concentration of 0.0583 mol/L. E_f increases with the increase of concentration or the decrease of injection rate, which takes the same trend with experiments. Manifested by Figure 13, the concentration changes obviously where interfacial convection occurs (Figure 13a) and the convection changes stronger with the increase of $c_{HAC,d}$ or the decrease of Q_{in} (Figure 13b).

According to Figure 12, the mass-transfer process during drop formation can be roughly divided into three periods. The extraction fraction increases noticeably during the first period, while E_f keeps almost at a same level or increases quite slowly during the second period, and finally E_f increases again when the necking stage begins (the third period). As illustrated by the numerical simulation (Figure 14), the first stage (static expansion stage) in the well-known two-stage drop formation hydrodynamic model (static expansion stage and necking stage)[67] should be divided into two mass-transfer periods: the first mass-transfer period when the length-to-width ratio of drop $h/w \leq 1$ and the second period when $h/w > 1$.

In the first period when $h/w \leq 1$, the vibration of the drop is unobvious as h/w presented in Figure 14 growing smoothly, and the Marangoni convection is directed from the dispersed phase to the continuous phase (Figure 13). At the beginning, the solute concentration difference across the interface is large (Figure 15), and thus the mass-transfer rate is high in the first period (Figure 16). With the development of the internal and external convections induced by Marangoni effect, the concentration boundary layer expands deeper into the bulk phase, which is difficult to be observed in experiments. As the solute transported by interfacial convection, the solute concentration around the interface inside the drop is much less than the drop bulk concentration, whereas the concentration outside the drop at the corresponding location is greater than the bulk concentration in the continuous phase. With the decline of the driving force for mass transfer, mass-transfer rates would decrease in the second period. On the contrary, there is no interfacial and internal convection when the interfacial tension set to be constant

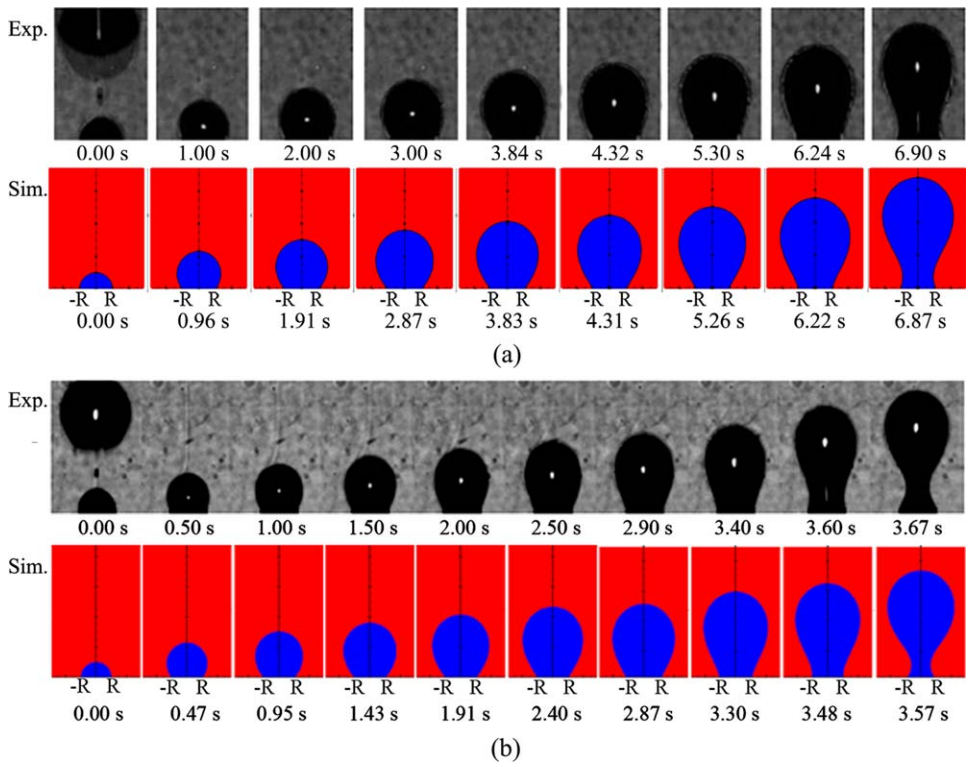

Figure 9. Comparison of experimental and simulated drop shapes during drop formation ($c_{HAC,d}$ = 0.0583 mol/L): (a) Q = 100 μL/min and (b) Q = 200 μL/min.

[Color figure can be viewed in the online issue, which is available at wileyonlinelibrary.com.]

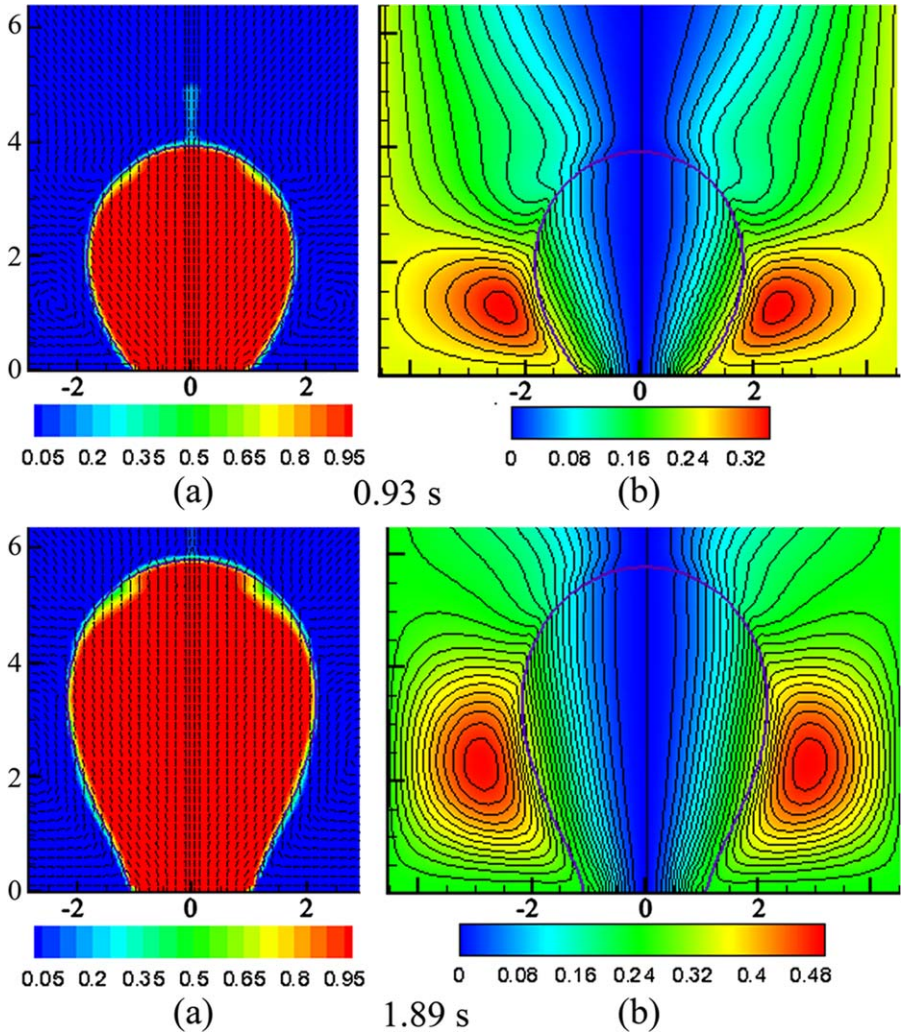

Figure 10. Predicted fractional solute concentration distribution and velocity vector field (a) and streamline contours (b) during drop formation (1-hexanol/acetic acid/water, constant interfacial tension $\sigma = 5.51$ mN/m at $c_{HAC,d} = 0.333$ mol/L, $Q = 366$ μL/min).

[Color figure can be viewed in the online issue, which is available at wileyonlinelibrary.com.]

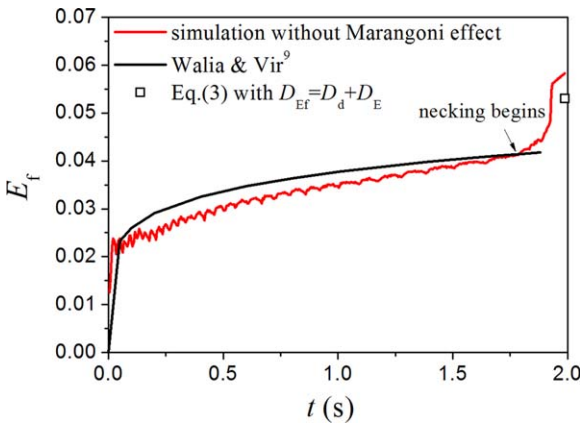

Figure 11. Comparison of simulated extraction fraction with prediction models during drop formation without Marangoni effect (1-hexanol/acetic acid/water, constant interfacial tension $\sigma = 5.51$ mN/m at $c_{HAC,d} = 0.333$ mol/L, $Q = 366$ μL/min).

[Color figure can be viewed in the online issue, which is available at wileyonlinelibrary.com.]

($\sigma = 5.51$ mN/m at $c_{HAC,d} = 0.333$ mol/L), the depth of concentration boundary layer except that at the head is less than 0.2 mm and changes negligibly with time. The mass-transfer rate does not change noticeably. That the extraction fraction when Marangoni effect occurs is higher than the case without Marangoni effect is resulted from that the mass-transfer rate during the first period is enhanced by Marangoni convection (Figure 16).

As seen from Figure 12, the extraction fraction even fluctuates down obviously during the second mass-transfer period. The mass-transfer measurement during drop formation by Wegener et al.[27] also indicated that the transferred mass did not increase with the drop size when Marangoni effect occurred (Table 2). In addition to the fluctuation of extraction fraction, we also found noticeable drop vibration in the second period. At the same time, as shown in Figure 17a, the drop height-to-width ratio with Marangoni effect is smaller than that with fixed σ in the simulation and the drop height-to-width ratio with Marangoni effect changes more noticeably. The change of flow pattern displayed in Figure 17b may help to explain the fluctuations. The concentration gradient gets larger with accumulation of solute on the drop's topside out of the interface, and a circulation cell taking fluid from the

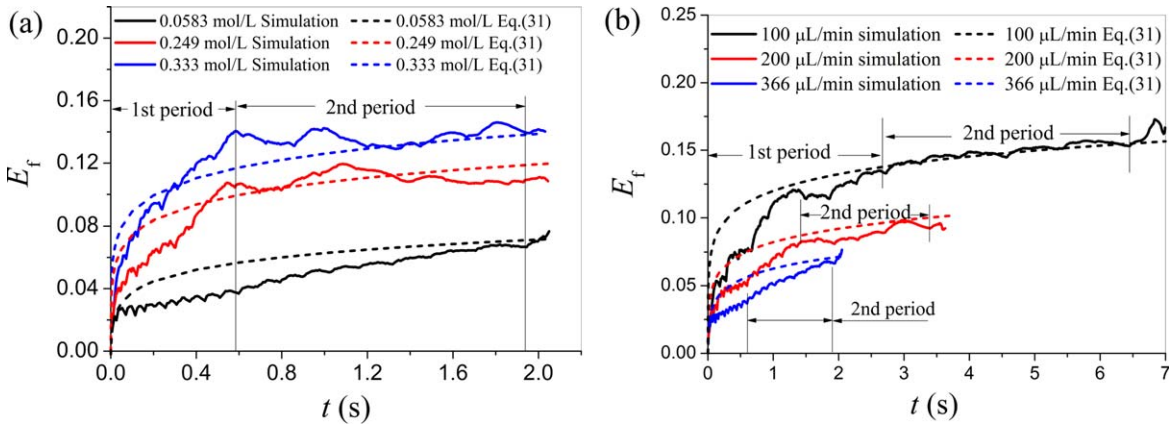

Figure 12. Simulated transient extraction fractions at different initial solute concentrations ($Q = 366$ μL/min) (a) and at different formation rates ($c_{HAC} = 0.0583$ mol/L) (b).

[Color figure can be viewed in the online issue, which is available at wileyonlinelibrary.om.]

continuous phase to the drop phase develops at the top at 0.9796 s as marked by a square box in Figure 17b. As some of the solute should be carried by the convection from the continuous phase to the dispersed phase, the extraction fraction decreases in the time interval of 0.9508 to 0.9796 s. Meanwhile, the fluid downward movement developed at the interface makes the drop expanded in the radial direction and the internal circulation developed. With more solutes taken by the internal circulation to the interface, the extraction fraction increases from 0.9796 to 0.9988 s, and the solute concentration gradient in the circulation cell may be reduced. With the diminishment of internal circulation and the development of the back-mixing mode convection from the continuous phase to the dispersed phase (inside the square marker at 1.0276 s), the extraction fraction decreases again.

Conclusions

The Marangoni effect induced by the mass transfer during drop formation was investigated experimentally and

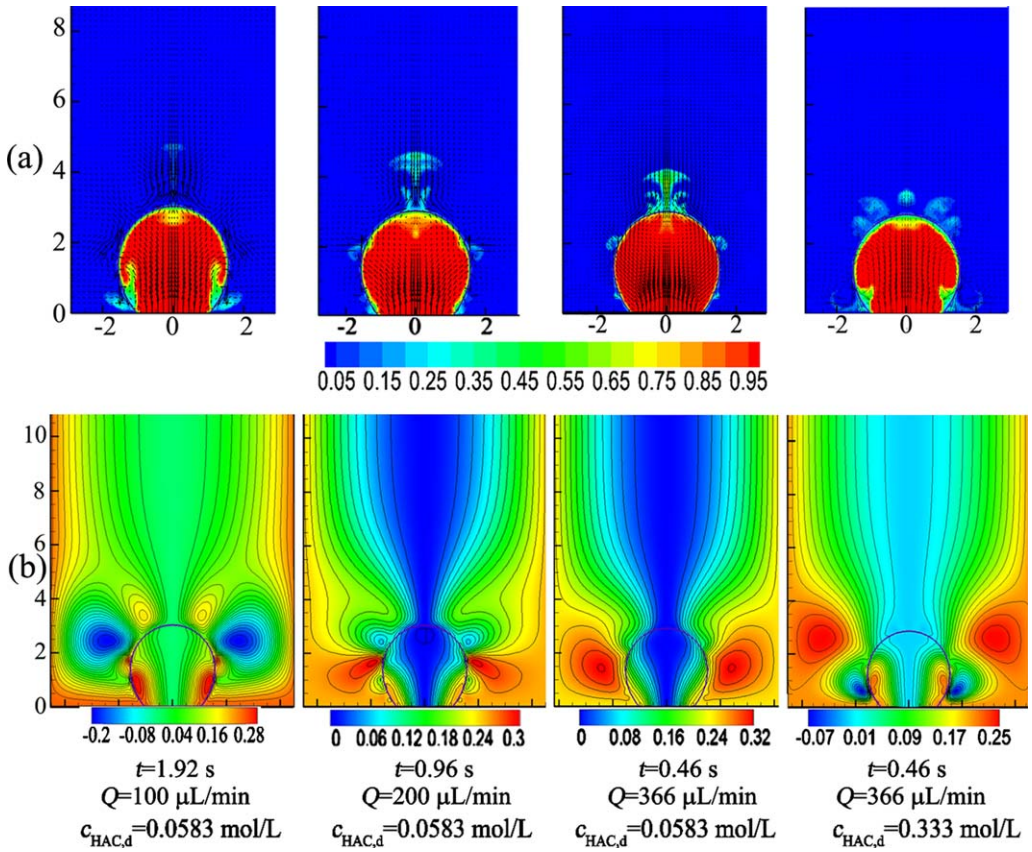

Figure 13. Predicted fractional solute concentration distribution and velocity vector field (a) and streamline contours (b).

[Color figure can be viewed in the online issue, which is available at wileyonlinelibrary.com.]

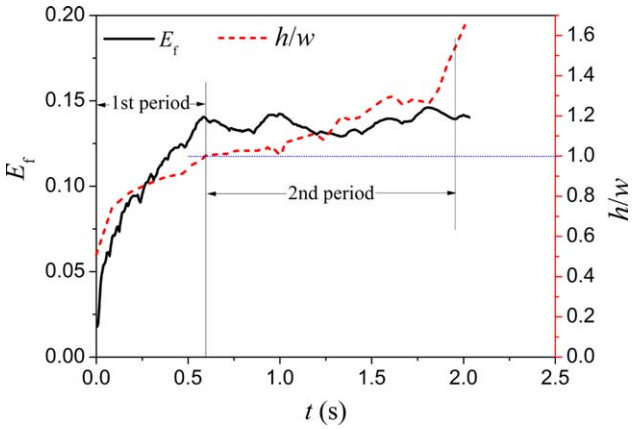

Figure 14. The division of the first and second periods in the mass-transfer process during drop formation ($c_{HAC,d}$ = 0.333 mol/L, Q = 366 μL/min).

[Color figure can be viewed in the online issue, which is available at wileyonlinelibrary.com.]

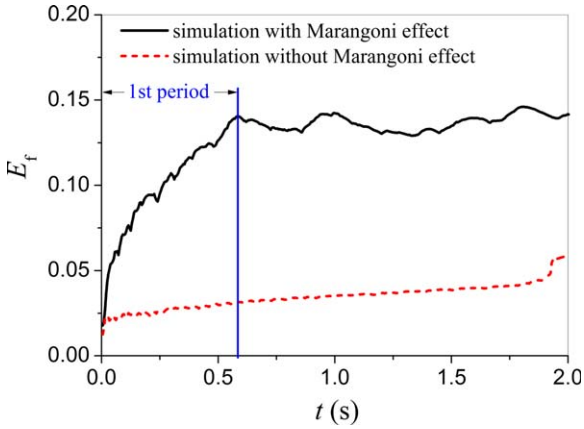

Figure 16. Comparison of simulated extraction fractions with Marangoni effect and without Marangoni effect ($c_{HAC,d}$ = 0.333 mol/L, Q = 366 μL/min).

[Color figure can be viewed in the online issue, which is available at wileyonlinelibrary.com.]

numerically. Marangoni convections became stronger with the increase of initial concentrations or the decrease of injection flow rates. Marangoni instability during drop formation can enhance mass transfer efficiently. By accounting for Marangoni effect, viscosity, and convective effect, a correlation to estimate the extraction fraction during drop formation accompanied with Marangoni instability was proposed.

The level-set method coupled with mass-transfer equation is first used to simulate the Marangoni effect induced by interphase mass transfer during the drop formation stage. The numerical model with a proper mass-amending technique can predict well the hydrodynamics of drop formation. The predicted extraction fractions, both with and without Marangoni effect, agree well with experimental data, indicating that the mathematical model and numerical method can simulate effectively the Marangoni effect during drop formation. According to the numerical simulation, when Marangoni convection occurs, the mass-transfer period can be roughly divided into three periods according to the change of mass-transfer rates, and the division between the first period and the second period coincides with that of the height-to-width ratio of a drop (h/w = 1). The mass transfer in the first period during drop formation was enhanced noticeably by Marangoni effect. During the second period, the extraction fraction may be reduced when the solute is

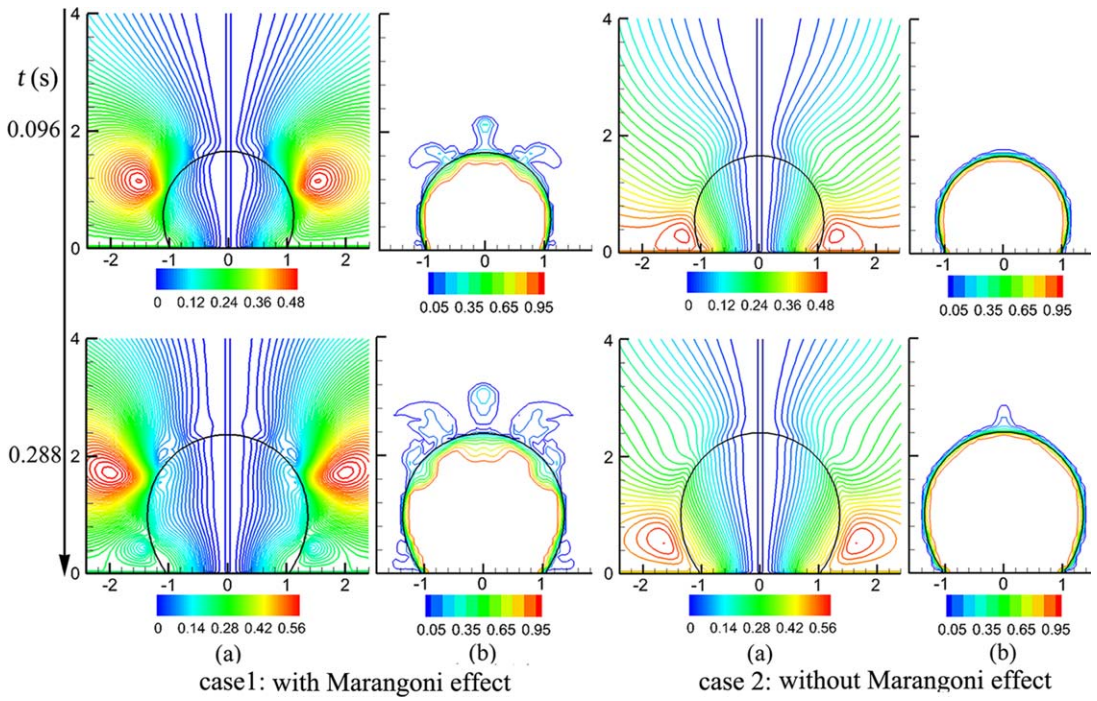

Figure 15. Evolution of flow patterns (a) and concentration contours (b) ($c_{HAC,d}$ = 0.333 mol/L, Q = 366 μL/min, Case 1 with Marangoni effect, Case 2 without Marangoni effect).

[Color figure can be viewed in the online issue, which is available at wileyonlinelibrary.com.]

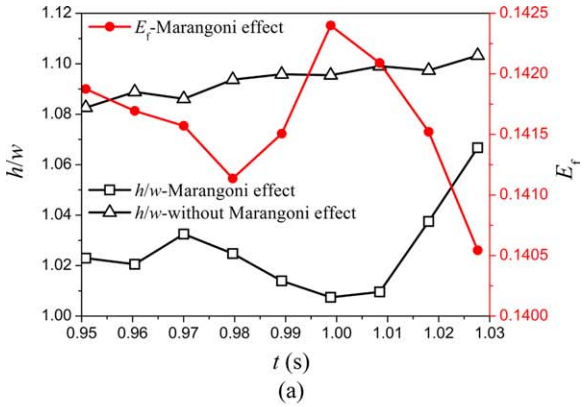

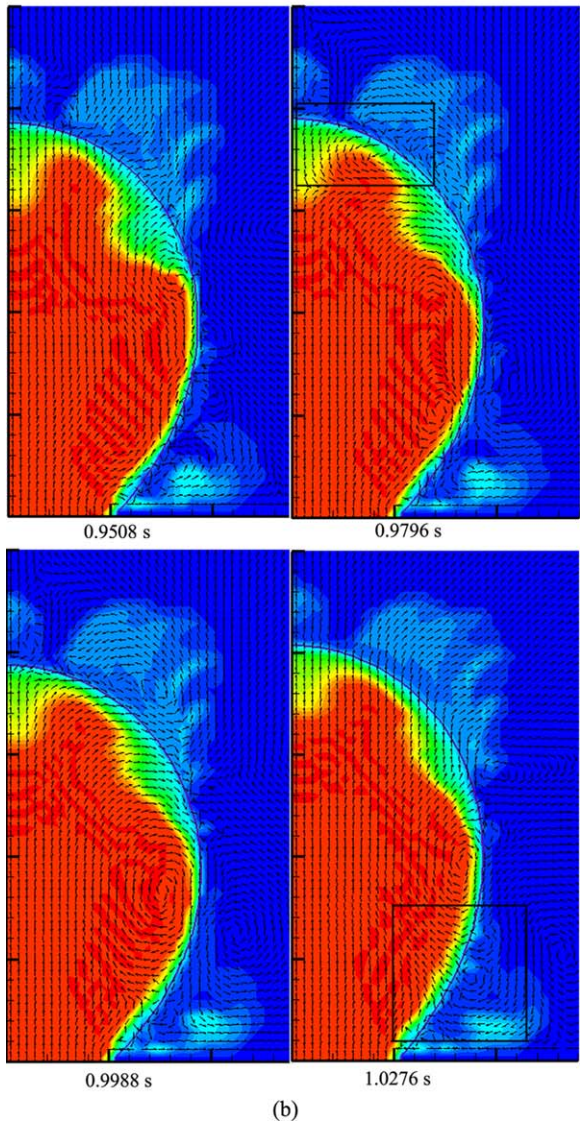

Figure 17. Change of drop height-to-width ratios (*h/w*) (a) and flow patterns (b) during drop formation: $c_{HAC,d}$ = 0.333 mol/L, *Q* = 366 μL/min.

[Color figure can be viewed in the online issue, which is available at wileyonlinelibrary.com.]

transported by the interfacial convection flowing from the continuous phase to the dispersed phase simultaneously with the vibration of drops.

Acknowledgments

Financial supports from 973 Program (2012CB224806), the National Natural Science Foundation of China (21106150, 20990224), the National Science Fund for Distinguished Young Scholars (21025627) and 863 project (2012AA03A606) are gratefully acknowledged.

Notation

A = mass of a drop, kg
c_0 = initial concentration, mol/L
c_f = concentration of collected drops, mol/L
$c_{HAC,d}$ = initial concentration of acetic acid in dispersed phase, mol/L
c^* = concentration in equilibrium with other phase, mol/L
C = dimensionless concentration
$\hat{C}$ = transformed concentration in mass-transfer equation
d = equivalent spherical diameter of a drop during formation, mm
d_f = final equivalent spherical diameter of a drop, mm
d_N = nozzle diameter, mm
D = diffusion coefficient, m^2/s
D_{Ef} = effective diffusion coefficient, m^2/s
$\hat{D}$ = transformed diffusion coefficient in mass-transfer equation
E_c = constant in Eq. 20
E_f = extraction fraction
$E_{f,tot}$ = extraction fraction accounting for coalescence in Eq. 27
$E_{f,det}$ = extraction fraction at detachment time in Eq. 36
Fo = Fourier number, $Fo=tD_{Ef}/d_f^2$
$\mathbf{F}_{Ma}$ = Marangoni force, N/m^3
g = acceleration vector of gravity, $9.81 m/s^2$
h = height of a drop
k = mass-transfer coefficient, m/s
m = equilibrium coefficient
Ma = Marangoni number, $Ma=d_f\Delta\sigma/(\mu_d D_d)$
n = unit vector normal to surface
P = pressure, Pa
r = radial coordinate, m
R = radius of a drop, m
R_N = radius of nozzle, m
Re = Reynolds number, $Re=u_d\rho_d d/\mu_d$
Re_N = Reynolds number in the needle, $Re_N=\rho_d u_N d_N/\mu_d$
S = surface area of a drop, m^2
Sc = Schmidt number, $Sc=\mu_d/(\rho_d D_d)$
t = time, s
t_f = formation time, s
t_c = contact time, s
$\hat{t}$ = transformation time in mass-transfer equation
u = velocity vector, m/s
u = axial velocity component, m/s
u_d = average velocity in a drop, m/s
u_N = average velocity in the needle, m/s
v = radial or transverse velocity component, m/s
w = the widest diameter of a drop, m
We = Weber number, $We=(2R)^2 g\rho_c/\sigma$
x = axial coordination, m
y = radial or transverse coordination, m
$\boldsymbol{\tau}$ = stress tension, N/m^2
Δt = time step.

Greek

ε = finite ''thickness'' of the interface, m
κ = curvature of drop surface
μ = viscosity, Pa·s
μ_c = viscosity of continuous phase, Pa·s
μ_d = viscosity of dispersed phase, Pa·s
ρ = density, $kg\cdot m^{-3}$
ϕ = level-set function
σ = interfacial tension, N/m
τ = virtual time in a reinitialization or mass modification step.

Subscripts

d = dispersed phase
c = continuous phase
HAC = acetic acid
0 = initial
Pred. = prediction
Sim. = simulation.

Literature Cited

1. Popovich AT, Jervis RE, Trass O. Mass transfer during single drop formation. *Chem Eng Sci*. 1964;19:357–365.
2. Skelland AHP, Minhas SS. Dispersed phase mass transfer during drop formation and coalescence in liquid-liquid extraction. *AIChE J*. 1971;17:1316–1324.
3. Lee Y-L. Surfactants effects on mass transfer during drop-formation and drop falling stages. *AIChE J*. 2003;49:1859–1869.
4. Javadi A, Bastani D, Taeibi-Rahni M. Mass transfer during drop formation on the nozzle: new flow expansion model. *AIChE J*. 2006; 52:895–910.
5. Licht W, Conway JB. Mechanism of solute transfer in spray towers. *Ind Eng Chem.* 1950;42:1151–1157.
6. Coulson JM, Skinner SJ. The mechanism of liquid-liquid extraction across stationary and moving interfaces. 1. Mass transfer into single dispersed drops. *Chem Eng Sci*. 1952;1:197–211.
7. Heertjes PM, de Nie LH. The mechanism of mass transfer during formation, release and coalescence of drops. Part I—mass transfer to drops formed at a moderate speed. *Chem Eng Sci*. 1966;21:755–768.
8. Walia DS, Vir D. Extraction from single forming drops. *Chem Eng J*. 1976;12:133–141.
9. Walia DS, Vir D. Interphase mass transfer during drop or bubble formation. *Chem Eng Sci*. 1976;31:525–533.
10. Liang T-B, Slater MJ. Liquid-liquid extraction drop formation: mass transfer and the influence of surfactant. *Chem Eng Sci*. 1990;45:91–105.
11. Handlos AE, Baron T. Mass and heat transfer from drops in liquid-liquid extraction. *AIChE J*. 1957;3:127–136.
12. Lu P, Wang ZH, Yang C, Mao Z-S. Experimental investigation and numerical simulation of mass transfer during drop formation. *Chem Eng Sci*. 2010;65:5517–5526.
13. Zimmermann V, Halwachs W, Schugerl K. Mass transfer investigations during droplet formation by means of a modified liquid scintillation technique. *Chem Eng Commun.* 1980;7:95–112.
14. Arendt B, Eggers R. Interaction of marangoni convection with mass transfer effects at droplets. *Int J Heat Mass Transfer*. 2007;50:2805–2815.
15. Henschke M, Pfennig A. Mass-transfer enhancement in single-drop extraction experiments. *AIChE J*. 1999;45:2079–2086.
16. Schwabe D, Hintz P, Frank S. New features of thermocapillary convection in floating zones revealed by tracer particle accumulation structures (PAS). *Microgravity Sci Technol*. 1996;9:163–168.
17. Schwabe D. The Benard-Marangoni-instability in Small Circular Containers under Microgravity: Experimental Results, in Gravitational Effects in Materials and Fluid Sciences. Oxford: Pergamon Press Ltd., 1999:1347–1356.
18. Yang WJ. Handbook of Flow Visualization. New York: Hemisphere Pub. Corp., 1989:189–201.
19. Okhotsimskii A, Hozawa M. Schlieren visualization of natural convection in binary gas-liquid systems. *Chem Eng Sci*. 1998;53:2547–2573.
20. Lohner H, Czisch C, Lehmann P, Bauckhage K. Mass transfer processes in liquid-liquid systems with surfactants. *Chem Eng Technol*. 2001;24:1157–1163.
21. Agble D, Mendes-Tatsis MA. The effect of surfactants on interfacial mass transfer in binary liquid-liquid systems. *Int J Heat Mass Transfer*. 2000;43:1025–1034.
22. Arendt B, Dittmar D, Eggers R. Interaction of interfacial convection and mass transfer effects in the system co_2–water. *Int J Heat Mass Transfer*. 2004;47:3649–3657.
23. Hozawa M, Shoji K, Tadaki T. Effect of rayleigh instability on gas absorption rate. *Int Chem Eng*. 1976;16:341–346.
24. Kronig R, Brink JC. On the theory of extraction from droplets. *Appl Sci Res*. 1950;A2:142–147.
25. Wang ZH, Lu P, Zhang G, Yong Y, Yang C, Mao Z-S. Experimental investigation of Marangoni effect in 1-hexanol/water system. *Chem Eng Sci*. 2011;66:2883–2887.
26. Javadi A, Bastani D, Kraegel J, Miller R. Interfacial instability of growing drop: experimental study and conceptual analysis. *Colloid Surf A Physicochem Eng Asp*. 2009;347:167–174.
27. Wegener M, Paschedag AR, Kraume M. Mass transfer enhancement through Marangoni instabilities during single drop formation. *Int J Heat Mass Transfer*. 2009;52:2673–2677.
28. Leshansky AM, Nir A. Thermocapillary alignment of gas bubbles induced by convective transport. *J Colloid Interface Sci*. 2001;240: 544–551.
29. Leshansky AM, Lavrenteva OM, Nir A. Thermocapillary migration of bubbles: convective effects at low peclet number. *J Fluid Mech*. 2001;443:377–401.
30. Nas S, Tryggvason G. Thermocapillary interaction of two bubbles or drops. *Int J Multiphase Flow*. 2003;29:1117–1135.
31. Zhou H, Davis RH. Axisymmetric thermocapillary migration of two deformable viscous drops. *J Colloid Interface Sci*. 1996;181:60–72.
32. Berejnov V, Leshansky AM, Lavrenteva OM, Nir A. Spontaneous thermocapillary interaction of drops: effect of surface deformation at nonzero capillary number. *Phys Fluids*. 2002;14:1326–1339.
33. Rother MA, Zinchenko AZ, Davis RH. A three-dimensional boundary-integral algorithm for thermocapillary motion of deformable drops. *J Colloid Interface Sci*. 2002;245:356–364.
34. Yin Z-H, Chang L, Hu W-R, Gao P. Thermocapillary migration and interaction of two nondeformable drops. *Appl Math Mech Engl Ed*. 2011;32:811–824.
35. Liu H, Zhang Y, Valocchi AJ. Modeling and simulation of thermocapillary flows using lattice boltzmann method. *J Comput Phys*. 2012;231:4433–4453.
36. Lappa M, Savino R, Monti R. Three-dimensional simulation of marangoni instabilities in non-cylindrical liquid bridges in microgravity. *Int J Heat Mass Transfer*. 2001;44:1983–2003.
37. Li J, Li MW, Hu WR, Zeng DL. Suppression of marangoni convection of silicon melt by a non-contaminating method. *Int J Heat Mass Transfer*. 2003;46:4969–4973.
38. Kahouadji L, Houchens BC, Witkowski LM. Thermocapillary instabilities in a laterally heated liquid bridge with end wall rotation. *Phys Fluids*. 2011;23:1041041–10410416.
39. Bouizi O, Delcarte C, Kasperski G. Stability study of the floating zone with respect to the prandtl number value. *Phys Fluids*. 2007; 19:1141021–11410212.
40. Lee CH, Ha JJ, Chun BH, Yoon HK, Kim SH. Mathematical modeling and simulation for marangoni convection by surfactants in liquid failing film. *J Chem Eng Jpn*. 2003;36:259–264.
41. Bratsun DA, De Wit A. On marangoni convective patterns driven by an exothermic chemical reaction in two-layer systems. *Phys Fluids*. 2004;16:1082–1096.
42. Grahn A. Two-dimensional numerical simulations of marangoni-benard instabilities during liquid-liquid mass transfer in a vertical gap. *Chem Eng Sci*. 2006;61:3586–3592.
43. Viviani A, Zuev A. Deformation and rupture of a horizontal liquid layer by thermal and solutal marangoni flows. *Energy Convers Manag*. 2008;49:3232–3236.
44. Mao Z-S, Lu P, Zhang GJ, Yang C. Numerical simulation of the marangoni effect with interphase mass transfer between two planar liquid layers. *Chin J Chem Eng*. 2008;16:161–170.
45. Sun ZF. Onset of rayleigh–bénard–marangoni convection with time-dependent nonlinear concentration profiles. *Chem Eng Sci*. 2012;68: 579–594.
46. Schott R, Pfennig A. Modelling of mass-transfer induced instabilities at liquid–liquid interfaces based on molecular simulations. *Mol Phys*. 2004;102:331–339.
47. Mao Z-S, Chen JY. Numerical simulation of the marangoni effect on mass transfer to single slowly moving drops in the liquid-liquid system. *Chem Eng Sci*. 2004;59:1815–1828.
48. Wang JF, Yang C, Mao Z-S. Numerical simulation of marangoni effects of single drops induced by interphase mass transfer in liquid-liquid extraction systems by the level set method. *Sci China B Chem*. 2008;51:684–694.
49. Wang JF, Wang ZH, Lu P, Yang C, Mao Z-S. Numerical simulation of the marangoni effect on transient mass transfer from single moving deformable drops. *AIChE J*. 2011;57:2670–2683.
50. Wegener M, Eppinger T, Baumler K, Kraume M, Paschedag AR, Bansch E. Transient rise velocity and mass transfer of a single drop with interfacial instabilities-numerical investigations. *Chem Eng Sci*. 2009;64:4835–4845.
51. Ohta M, Yamamoto M, Suzuki M. Numerical analysis of a single drop formation process under pressure pulse condition. *Chem Eng Sci*. 1995;50:2923–2931.
52. Zhang X. Dynamics of drop formation in viscous flows. *Chem Eng Sci*. 1999;54:1759–1774.
53. Gerlach D, Alleborn N, Buwa V, Durst F. Numerical simulation of periodic bubble formation at a submerged orifice with constant gas flow rate. *Chem Eng Sci*. 2007;62:2109–2125.
54. Buwa V, Gerlach D, Durst F, Schlucker E. Numerical simulations of bubble formation on submerged orifices: period-1 and period-2 bubbling regimes. *Chem Eng Sci*. 2007;62:7119–7123.

55. Soleymani A, Laari A, Turunen I. Simulation of drop formation in a single hole in solvent extraction using the volume-of-fluid method. *Chem Eng Res Des*. 2008;86:731–738.
56. Chen Y, Mertz R, Kulenovic R. Numerical simulation of bubble formation on orifice plates with a moving contact line. *Int J Multiphase Flow*. 2009;35:66–77.
57. Yang C, Lu P, Mao Z-S, Yu GZ, Zhang GJ, Chen JY. Numerical simulation of hydrodynamics of drop formation by a level set method. *J Nanjing Univ Technol*. 2006;28:27–33.
58. Wilke CR, Chang P. Correlation of diffusion coefficients in dilute solutions. *AIChE J*. 1955;1:264–270.
59. Misek T. Recommended Systems for Liquid Extraction Studies, EFCE publications series. Rugby, UK: Institute of Chemical Engineers, 1978.
60. Brackbill JU, Kothe DB, Zemach CA. A continuum method modeling surface tension. *J Comput Phys*. 1992;101:335–354.
61. Wang JF, Yang C, Mao Z. A simple weighted integration method for calculating surface tension force to suppress parasitic flow in the level set approach. *Chin J Chem Eng*. 2006;14:740–746.
62. Yang C, Mao Z-S. Numerical simulation of interphase mass transfer with the level set approach. *Chem Eng Sci*. 2005;60:2643–2660.
63. Sussman M, Smereka P, Osher S. A level set approach for computing solutions to incompressible two-phase flow. *J Comput Phys*. 1994;114:146–159.
64. Chang YC, Hou TY, Merriman B, Osher S. A level set formulation of eulerian interface capturing methods for incompressible fluid flows. *J Comput Phys*. 1996;124:449–464.
65. Yang C, Mao Z-S. An improved level set approach to the simulation of drop and bubble motion. *Chin J Chem Eng*. 2002;10:263–272.
66. Zhang H, Zheng LL, Prasad V, Hou TY. A curvilinear level set formulation for highly deformable free surface problems with application to solidification. *Numer Heat Transfer B* 1998;34:1–20.
67. Scheele GF, Meister BJ. Drop formation at low velocities in liquid-liquid systems: part I. *Prediction of drop volume*. *AIChE J*. 1968;14:9–19.
68. Kovalchuk NM, Vollhardt D. Marangoni instability and spontaneous non-linear oscillations produced at liquid interfaces by surfactant transfer. *Adv Colloid Interface Sci*. 2006;120:1–31.

Manuscript received Jan. 27, 2013, and revision received Apr. 25, 2013.